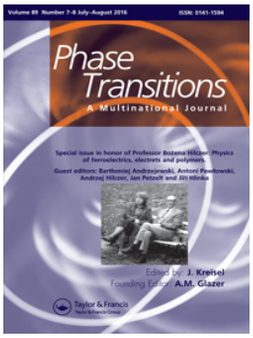

Taylor & Francis
Taylor & Francis Group

Phase Transitions
A Multinational Journal

ISSN: 0141-1594 (Print) 1029-0338 (Online) Journal homepage: https://www.tandfonline.com/loi/gpht20

New features from transparent thin films of $EuTiO_3$

B. Stuhlhofer, G. Logvenov, M. Górny, K. Roleder, A. Boris, D. Pröpper, R. K. Kremer, J. Köhler & A. Bussmann-Holder

To cite this article: B. Stuhlhofer, G. Logvenov, M. Górny, K. Roleder, A. Boris, D. Pröpper, R. K. Kremer, J. Köhler & A. Bussmann-Holder (2016) New features from transparent thin films of $EuTiO_3$, Phase Transitions, 89:7-8, 731-739, DOI: 10.1080/01411594.2016.1199805

To link to this article: https://doi.org/10.1080/01411594.2016.1199805

Published online: 05 Jul 2016.

PHASE TRANSITIONS, 2016
VOL. 89, NOS. 7–8, 731–739
http://dx.doi.org/10.1080/01411594.2016.1199805

Taylor & Francis
Taylor & Francis Group

New features from transparent thin films of $EuTiO_3$

B. Stuhlhofer[a], G. Logvenov[a], M. Górny[b]†, K. Roleder[b], A. Boris[a], D. Pröpper[a], R. K. Kremer[a], J. Köhler[a] and A. Bussmann-Holder[a]

[a]Max-Planck-Institut für Festkörperforschung, Stuttgart, Germany; [b]Institute of Physics, University of Silesia, Katowice, Poland

ABSTRACT

The almost multiferroic perovskite $EuTiO_3$ (ETO) has been prepared as films on substrates of $SrTiO_3$. For all prepared film thicknesses highly transparent insulating films with atomically flat surfaces and excellent orientation have been grown. They were characterized by X-ray diffraction, magnetic susceptibility and birefringence measurements and found to exhibit bulk properties, namely an antiferromagnetic transition at $T_N = 5.1$ K and a structural transition at $T_S = 282$ K. The latter could only be identified due to the high transparency of the samples since the optical band gap is of the order of 4.5 eV and larger than observed before for any bulk and thin film samples.

ARTICLE HISTORY
Received 9 May 2016
Accepted 3 June 2016

KEYWORDS
Phase transitions; $EuTiO_3$; antiferrromagnetism; birefringence

PACS-INDEX
75.70.-i; 77.55.Nv; 63.70.+h

1. Introduction

$EuTiO_3$ has been discovered early on,[1] but long been ignored scientifically since only its antiferromagnetic properties below $T_N = 5.5$ K were known.[2] The discovery of a strong magneto-dielectric effect at low temperatures [3] has revived the research in this field, expecting multiferroic properties to be realized in this material.[4] However, for the bulk material an extrapolation of the soft mode frequency to zero indicates a ferroelectric transition temperature around −170 K,[5,6] thus inconsistent with multiferroicity. Nevertheless, a tuning of the permittivity by a magnetic field reveals that ETO is a strong coupling magneto-dielectric compound.

Since thin film technology enables to include tensile and compressive strain to enhance multifunctionality in many oxides, attempts have been made to realize with these techniques the desired properties. Indeed, it was reported [7] that [001]-oriented ETO films on $DyScO_3$ substrates with 1.1% tensile strain exhibit high-temperature ferroelectricity combined with low-temperature ferromagnetism. Conclusions on these properties have been derived indirectly by means of second harmonic generation since leakage currents inhibited direct measurements of the spontaneous polarization. Ferromagnetism was detected below 4.3 K with a strongly reduced magnetization of only 3 μ_B/Eu in contrast to the expected one of 6.8 μ_B/Eu. The dielectric constant peak around 250 K, which was observed in those films, has been attributed to a possible ferroelectric phase transition, but could also be a consequence of the nearby structural phase transition, discovered later.[8]

A variety of other approaches to thin film manipulation on diverse substrates have been carried out [9–15] where, however, leakage was the central problem. Also, it was almost always observed that ETO films grown on STO in the as-grown state exhibit considerable *c*-axis shrinkage or expansion as compared to bulk samples.[8–12,14] This difference has been attributed to out-of-plane strain caused

CONTACT A. Bussmann-Holder a.bussmann-holder@fkf.mpg.de
† deceased

during vacuum annealing, and has been removed by post-annealing the samples. The major problem in thin film preparation relates, however, to the above-mentioned leakage currents which render it impossible to measure the polarization or permittivity directly. Also, there is no report, so far, on the unambiguous observation of the structural phase transition of ETO in thin films.

2. Experimental

For these reasons we have prepared thin films of ETO on substrates of $SrTiO_3$. Epitaxial $EuTiO_3$ (ETO) single crystalline films were synthesized by using pulsed laser deposition (PLD) process from the ETO polycrystalline target. The excellent quality of the films is not only a result of the careful PLD ablation process but also due to the target quality. The ETO target used here differs from others since the ETO samples were synthesized by repeatedly heating mixtures of Ti_2O_3 and Eu_2O_3 at 1300 °C with intimate grinding in between, which ensures optimal target properties.[8] The films were grown on $SrTiO_3$ [001] (STO) single crystal substrates provided by Crystec Company (Germany). For the PLD ablation process a KrF excimer laser with a wave length of 248 nm was used. The energy density on the target was ~1.6 J/cm^2 and the frequency of the pulsed laser beam was 10 Hz. The deposition rate was ~0.257 Å/pulse and was calibrated by measuring the film thickness with a profilometer. The substrate was heated by a resistive heater and kept constant during the film growth at 600 °C according to the radiation pyrometer reading. During the film deposition we maintained an oxygen flow with a flow rate 4.4 sccm, while the pressure in the deposition chamber was 1×10^{-5} mbar.

Films of various thicknesses (50, 100, 257, 500, and 1000 nm) were grown always on STO substrates, however, also with varying substrate thicknesses (1−0.1 mm) and were always highly transparent (Figure 1(a)) with resistivities larger than 100 MΩ. They were characterized by scanning electron microscopy (SEM) (Figure 1(b)) showing a smooth and homogenous surface, atomic force microscopy (AFM) (Figure 1(c)) evidencing a surface roughness of less than 0.25 nm and X-ray diffraction (Cu Kα_1 radiation) (Figure 1(d)). It is remarkable that the widths of reflections of our samples are very narrow and free from fringes most likely due to the rather large sample thickness. No features could be resolved which would be consistent with a *c*-axis shrinkage or expansion. Marginal differences between the lattice constants of ETO and STO appear upon blowing up the data and are consistent with the reported lattice parameters. From these data it is concluded that all films are cubic at room temperature and strain free.

3. Results

The low-temperature magnetic properties of thin films investigated so far differ significantly from bulk materials reporting ferromagnetism below 5 K in c-axis expanded samples.[16−20] In order to characterize the low-temperature magnetic properties of our films, the temperature dependence of the magnetic moment m was measured using a SQUID magnetometer (Quantum Design MPMS-XL). The data have been corrected for the diamagnetic background stemming from the STO substrate by measuring the substrate separately and subtracting these data from the ones of substrate plus film. The magnetic susceptibility was measured in two modes, namely in plane and perpendicular to the film. In both orientations an anomaly at $T_N = 5.1$ K was observed consistent with antiferromagnetic order and with previously obtained results,[16−20] however, slightly smaller than observed in our best ceramics with $T_N = 5.7$ K.[8] For the in-plane measurements the anomaly at T_N was less well resolved, as compared to the perpendicular mode configuration. Typical data corrected for the substrate in comparison to results obtained for bulk ceramic samples are shown in Figure 2.

We used spectroscopic ellipsometry to determine the optical band gap in ETO. Room temperature ellipsometric spectra in the spectral range from 0.6 to 6.5 eV were measured on a ~500-nm-thick ETO film at several angles of incidence (63°−75°) with a J.A. Woollam Co. VASE variable

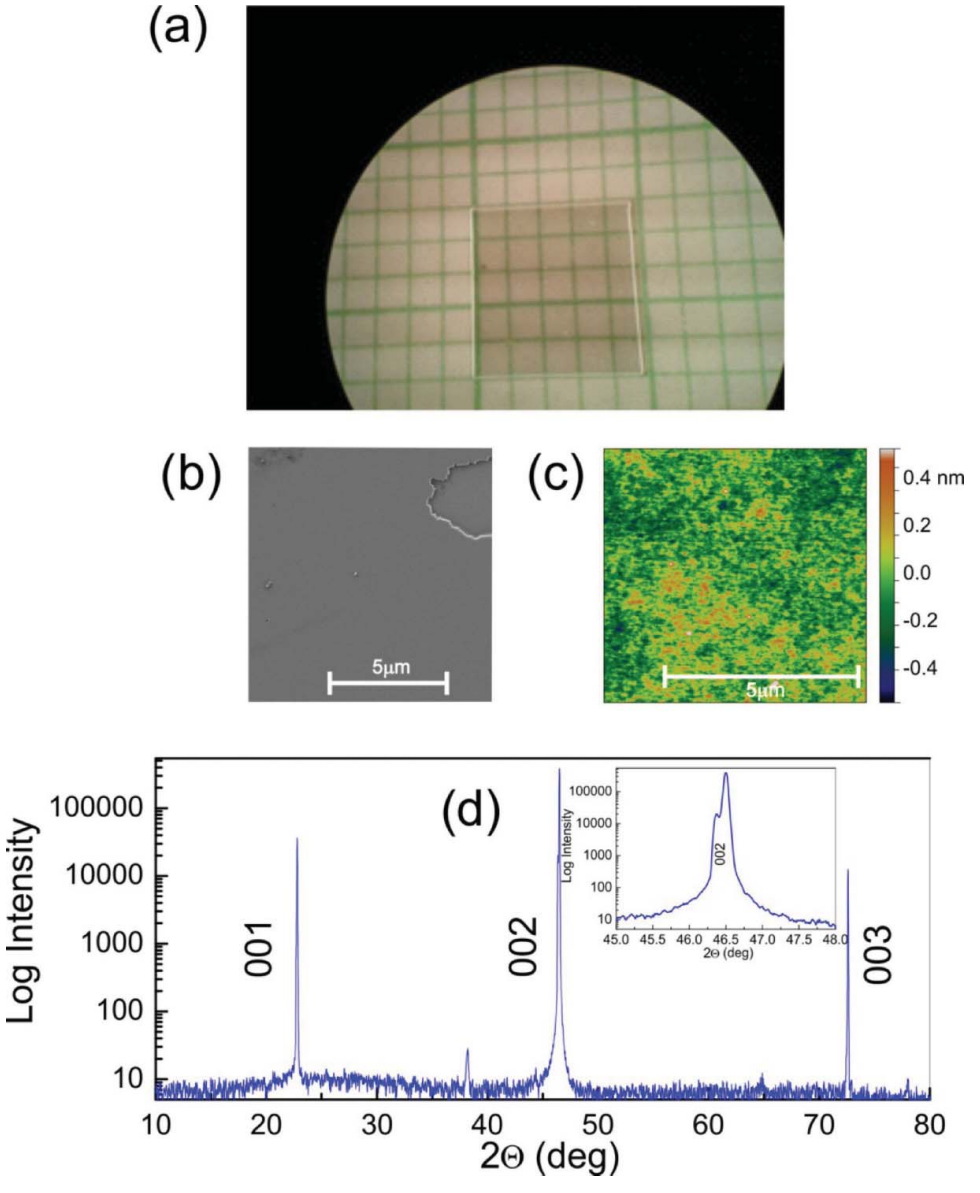

Figure 1. (a) Typical photograph of a 0.5 × 0.5 cm^2 ETO film. (b) and (c) Scanning electron microcopy SEM image and atomic force microscopy (AFM) image showing roughness of a selected area of the ETO film shown in (a), respectively. (d) XRD pattern of the ETO film on an STO substrate. The 38.2° Bragg peak stems from the sample holder. The inset shows a splitting of ∼0.12° of the [002] reflection indicating the slightly different lattice constants of ETO and STO.

angle spectroscopic ellipsometer. A numerical regression procedure [21,22] based on a three-layer optical model (consisting of 0.1-mm-thick STO substrate, ETO film and surface roughness layers) has been employed to extract the complex dielectric function of the ETO film. The thickness of the film and surface roughness layers (the letter was treated as a 50% bulk ETO film and 50% void mixture) were determined to be 482 ± 2 nm and 5.1 ± 0.4 nm, respectively. Figure 3 shows the real $\varepsilon_1(\omega)$ and imaginary $\varepsilon_2(\omega)$ parts of the dielectric function of ETO, compared with the dielectric function of STO used for the parametrized model. For ETO, a direct band gap of 4.53 ± 0.07 eV is obtained (inset to Figure 3) by the intersection of the line fitted to $(\varepsilon_2\ \omega^2)^2$ and the energy axis. [23,24]

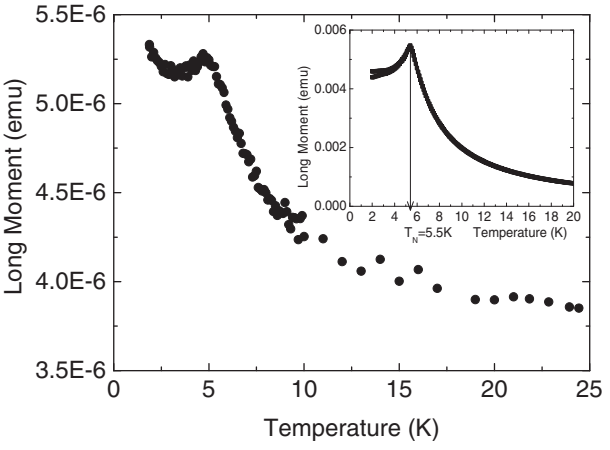

Figure 2. Magnetic moment in an external field of 0.1*T* as a function of temperature for a single crystalline film of ETO of thickness of 1000 nm measured with the field oriented perpendicular to the film. The inset shows the same, however, for bulk ceramic samples.[8]

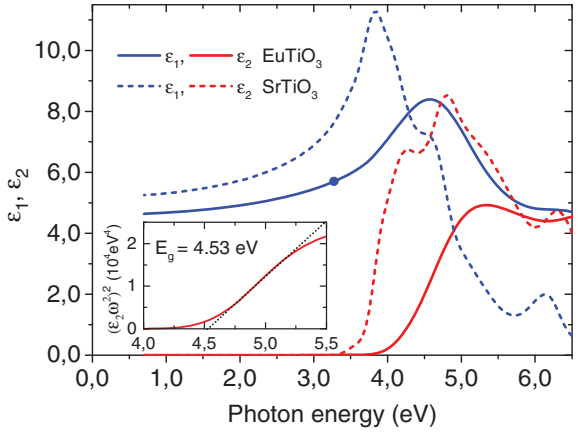

Figure 3. Real ε_1 (b) and imaginary ε_2 (r) parts of the complex dielectric function of $EuTiO_3$ (solid) and $SrTiO_3$ (dashed) at $T = 300$ K. Inset: Plot of $(\varepsilon_2\,\omega^2)^2$ for $EuTiO_3$ as a function of photon energy. The intercept of the dotted line with the energy axis defines the direct energy gap.

Another characteristic of ETO is its structural phase transition from cubic to tetragonal at $T_S = 282$ K [8] which has been debated in the literature, where values of T_S ranging from 130 to 310 K have been reported early after its discovery.[25–28] By improving the sample quality T_S has been limited to a narrow region around 282 K ± 8 K.[29–32] The detection of T_S is similarly difficult, as in STO,[33] since at low temperature the *c*/*a* ratio (1.0014) slightly deviates from one.[34] Specific heat, thermal expansion,[8,30] resonant ultrasound (RUS) [31,32] and muon spin rotation (μSR) measurements [35,36] all reveal clear anomalies related to T_S. Unfortunately these methods are hampered for our thin film samples due to the large background signal from the substrate. However, the high transparency of our samples admits to perform birefringence measurements which have already been successfully carried out on STO to identify its structural phase transition at $T_S = 105$ K.[37,38] These measurements together with the large resistivity and spectroscopic ellipsometry imply a band gap which is substantially larger than that of STO.

Birefringence measurements were made on an ETO film with thickness of 1 μm oriented in [100] direction and deposited on a single STO crystal substrate. The film and substrate together were of 85 μm thickness. The sample was placed in a high-precision Linkam TMSG600 temperature stage

combined with the birefringence imaging system.[37] The temperature was controlled to within ±0.1 K, and the measurements were made with cooling and heating rates of 0.5 K min^{-1}. Prior to performing the experiment, the sample was rejuvenated at a temperature of 470 K for half an hour. The Metripol Birefringence Imaging System (Oxford Cryosystems) consists of a polarizing microscope equipped with a computer-controlled plane-polarizer capable of being rotated to fixed angles α from a reference position, a circularly polarizing analyzer and a CCD camera. The intensity measured at any position is given by:

$$I = \frac{1}{2} I_0[1 + \sin(2\Phi - 2\alpha)\sin\delta]$$

where I_0 is the intensity of light that passes through the sample and represents its transmittance, Φ is the angle of an axis of the optical indicatrix of the specimen projected onto the image measured from a pre-determined direction, i.e. from the horizontal axis, and δ is the phase difference between the polarized light components, and is given by:

$$\delta = 2\pi^{-1}(n_1 - n_2)d,$$

where λ is the wavelength of the light, d is the thickness of the thin film and $\Delta n = (n_1 - n_2)$ is so-called plano-birefringence, i.e. the birefringence measured as seen in projection down the microscope axis. In all experiments the wavelength of 570 nm was used. Below the phase transition at $T_S = 282$ K from the cubic Pm-3m to tetragonal I4/mcm, the ETO film is in phase possessing a single optic axis. We have verified that the ETO film was oriented such that its z-axis, i.e. [001] direction of the tetragonal unit cell, was in plane of the surface of the substrate, and the main axis of the indicatrix was oriented 0° or 90° degree to the predetermined horizontal axis mentioned above. Hence, the measuring light beam passing through the ETO/STO sample was not parallel to the optic axis ([001] direction for the tetragonal symmetry), and the light was split into the ordinary and extraordinary ray. This set-up enabled us to observe the birefringence Δn. Since absolute values of Δn are determined by this method, the two orientations of the optic indicatrix were not an obstacle to obtain the temperature dependence of the birefringence. Because the film was of [100] orientation, the measuring light beam passing through the ETO/STO sample was not parallel to the optic axis (which is of [001] direction for the tetragonal symmetry), then the light was split into the ordinary and extraordinary ray, and thus the birefringence Δn could be observed.

By measuring several images with varying angle α, it is possible to fit for each pixel position the quantities I_0, sin δ and φ separately and then to plot images in false color representing these three values. In this way the birefringence can be detected with a very high sensitivity of the order of 10^{-6}. One of the interesting features of the Metripol system is the possibility to separate the birefringence of the sample from the effective retardation, which is a sum of true sample birefringence and the one stemming from the background. This effective retardation can be calculated according to the formula [37]:

$$\delta^* = \left\{ \left[\delta_m \sin(2\varphi_m) - \delta_b \sin(2\varphi_b)\right]^2 + \left[\delta_m \cos(2\varphi_m) - \delta_b \cos(2\varphi_b)\right]^2 \right\}^{\frac{1}{2}}$$

where $\delta_m = \sin^{-1}(|\sin\delta_m|)$ and φ_m are the phase shift and orientation angle measured in the ETO/STO sample, respectively, and $\delta_b = \sin^{-1}(|\sin\delta_b|)$ and φ_b are the phase shift and orientation angle measured as background values in the region outside the ETO/STO sample, respectively.

Figure 4 shows the temperature changes of the birefringence of ETO upon cooling and heating. These data are representative for tens of regions chosen for calculations of birefringence. Sizes of these regions varied from 50 × 50 μm^2 to 500 × 500 μm^2. Note that the birefringence of the STO substrate disappears above 150 K.[38] Up to 150 K the birefringence in STO is clearly temperature

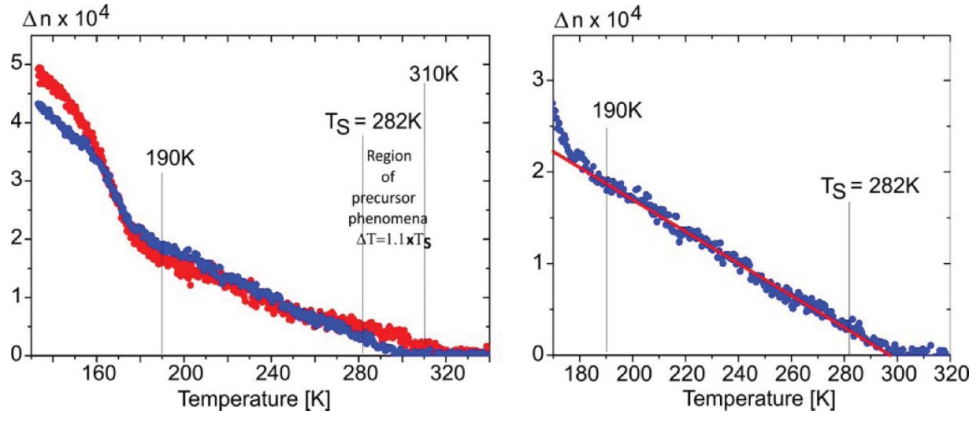

Figure 4. (Left) Birefringence Δn as a function of temperature in the range between 130 and 340 K. Above T_S clear precursor phenomena are present and correspond well to data in Figure 4. (Right) The straight line is a fit to the law $\Delta n \approx (T_S - T)^{2\beta}$ with $\beta = 0.5$ and $T_S = 297$ K, which point to the phase transition in ETO of a mean-field character with deviations from it starting below 190 K. T_S in the fit differs from that reported earlier and equal to 282 K.[39–42] This is probably because of micro-/nano-twinning with domains in ETO film evolving perpendicularly to the direction of light which may influence the slope of $\Delta n(T)$ run.

dependent and thus may produce local (non-homogenous) strains acting on the ETO film. For this reason we did not cool the sample far below 150 K.[38] In order to exclude any errors, birefringence experiments have been performed on the STO substrate only. These experiments on a 100-μm-thick STO single crystal confirmed that a non-zero birefringence, of the order of 2×10^{-6}, was observed in the temperature range from $T_S = 105$ K to approximately 160 K, while above 160 K no birefringence could be revealed.

In the investigated ETO/STO sample we did observe domain structure which could have an effect on the Δn values. This implies that we cannot exclude a domain structure which might evolve perpendicularly to the sample surface, namely, along the direction in which the light passes through the sample. In this case the measured value of Δn is an 'effective' one.

As is shown in Figure 4, above 190 K the linear $\Delta n(T)$ cooling and heating run in fact does not evidence a thermal hysteresis. Below 190 K $\Delta n(T)$ is nonlinear and shows a thermal hysteresis which may reflect the influence of the STO substrate caused by strain.

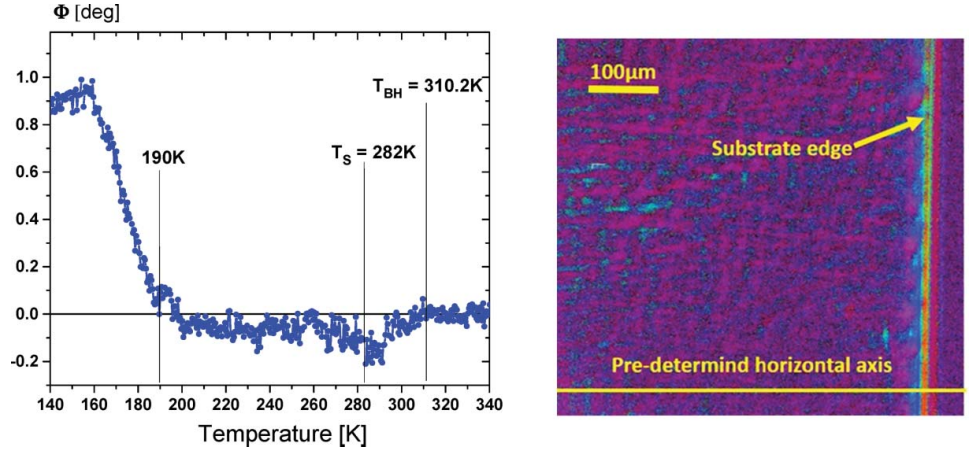

Figure 5. (Left) Temperature dependence of the discrepancy $\Delta\Phi$ of the optical indicatrix after background subtraction. T_{BH} is equal to $1.1 \times T_S$ and defines the limit of the existence of the precursor phenomenon above T_S of clusters with the symmetry of low-temperature phase. (Right) Light and bright (much less populated) regions represent domains in ETO film at 240 K (in the tetragonal phase) with optical indicatrix oriented 0° or 90° degree to the pre-determined horizontal direction, respectively.

Another evidence for the phase transition in ETO at 282 K is obtained from the temperature dependence of the discrepancy $\Delta\Phi$ (after background subtraction) of the angle between the main axis of the optical indicatrix and the predetermined horizontal axis (Figure 5, right). $\Delta\Phi$ clearly changes around 282 K (Figure 5, left), and before this transition temperature the precursor effect is distinctly observed. The temperature range of its existence has been calculated as $\Delta T = 1.1 * T_S - T_S = 28.2$ K. The origin of this precursor has been addressed [43] and is analogous to similar effects observed in other perovskites.[38]

Between 190 and 282 K the data can be well described by conventional Landau theory, where $\Delta n \approx (T_S - T)^{2\beta}$ with $\beta = 0.5$. This is analogous to STO,[37,38] but unlike STO the tetragonal domains are not observable due to domain wall pinning or freezing, consistent with RUS data. [31,32,44]

4. Conclusions

We conclude that our ETO films are of excellent quality because they are highly transparent with a band gap of 4.53 eV with AFM ordering below 5.1 K and $T_S = 282$ K. The band gap of 4.53 eV (Figure 3) is much larger than ever reported before.[45–49] Electronic structure calculations for ETO arrive at a band gap of 0.77 eV [47,48] which increases rapidly when Ti is replaced by Zr or Hf where in both latter compounds the gap is distinctly larger than 2eV. This large variation of the band gap in this series has been attributed to the transition metal d energy levels of the Ti 3d, Zr 4d and Hf 5d states which constitute the conduction bands and move to higher energy values with increasing principal quantum number. This result leads to a variety of inconsistencies with experimental data, as the nearest and next nearest neighbor exchange constants derived for this series cannot be explained with the band gap values. Also, the huge jump of the gap energy from the Ti compound to the Zr one [50] (1.6 eV) is difficult to explain by the increase in the principal quantum number.[51] Our new determination of the band gap of 4.53 eV removes the inconsistencies for the exchange constants mentioned above.

To summarize, we have successfully grown transparent ETO films on STO substrates of outstanding quality. The characterization of the films has evidenced that independent of the film thickness the samples become antiferromagnetic at $T_N = 5.1$ K. The transparency of all films together with spectroscopic ellipsometry data demonstrates that the band gap is much larger (4.53 eV) than ever reported. This is attributed to the absence of Ti^{3+} defect states which are present in previously investigated bulk and film samples. In addition, it allowed to detect the structural phase transition in thin films at $T_S = 282$ K by means of birefringence measurement with similar features as those observed in STO single crystals.

Acknowledgement

It is a pleasure to acknowledge Viola Duppel for recording the SEM image and Pirmin Ganter for providing the AFM image. Michał Górny passed away on January 18th, 2016. He was a high class specialist in the electronics and mechanics, and extremely talented experimentalist. It was a great pleasure to me to co-operate with him, and first of all to receive his help while modifying or constructing experimental setups. I was deeply impressed with his modest way of life and his readiness to help in laboratory work at any time he was asked for. The presence of his name in this paper is connected with his important contribution in modification of low temperature setup and with a very special tribute he deserves from my side (K.R.).

Disclosure statement

No potential conflict of interest was reported by the authors.

References

[1] Brous J, Fankuchen I, Banks E. Rare earth titanates with a perovskite structure. Acta Crystallogr. 1953;6:67–69.
[2] McGuire MTR, Shafer MW, Joenk RJ, et al. Magnetic structure of $EuTiO_3$. J Appl Phys. 1966;37:981–985.
[3] Katsufuji T, Takagi H. Coupling between magnetism and dielectric properties in quantum paraelectric $EuTiO_3$. Phys Rev B. 2001;64: 054415.
[4] Bussmann-Holder A, Köhler J. Revisiting the fascinating properties of $EuTiO_3$ and its mixed crystals with $SrTiO_3$: possible candidates for novel functionalities. J Phys Chem Solids. 2015;84:2–12.
[5] Kamba S, Nuzhnyy D, Vaněk P, et al. Magnetodielectric effect and optic soft mode behaviour in quantum paraelectric $EuTiO_3$ ceramics. Europhys Lett. 2007;80:27002.
[6] Goian V, Kamba S, Hlinka J, et al. Polar phonon mixing in magnetoelectric $EuTiO_3$. Eur Phys, J B. 2009;71: 429–436.
[7] Lee JH, Fang L, Vlahos E, et al. A strong ferroelectric ferromagnet created by means of spin-lattice coupling. Nature. 2010;466:954–958.
[8] Bussmann-Holder A, Köhler J, Kremer RK, et al. Lattice dynamical analogies and differences between $SrTiO_3$ and $EuTiO_3$ revealed by phonon-dispersion relations and double-well potentials. Phys Rev B. 2011;83:212102.
[9] Lee JH, Ke X, Podraza NJ, et al. Optical band gap and magnetic properties of unstrained $EuTiO_3$ films. Appl Phys Lett. 2009;94: 212509.
[10] Zong Y, Kugimiya K, Fujita K, et al. Preparation and magnetic properties of amorphous $EuTiO_3$ thin films. J Non-Cryst Solids. 2010;356:2389–2392.
[11] De Luca GM, Di Capua R, Di Gennaro E, et al. Transport properties of a quasi-two-dimensional electron system formed in $LaAlO_3/EuTiO_3/SrTiO_3$ heterostructures. Phys Rev B. 2014;89: 224413.
[12] Lv F, Zhang J, Gao C, et al. Hydrothermal epitaxy and resultant properties of $EuTiO_3$ films on $SrTiO_3$(001) substrate. Nanoscale Res Lett. 2014;9:266–271.
[13] Zhao R, Li WW, Chen L, et al. Conduction mechanisms of epitaxial $EuTiO_3$ thin films. Appl Phys Lett. 2012;101:102901.
[14] Goian V, Kamba S, Pacherová O, et al. Antiferrodistortive phase transition in $EuTiO_3$. Phys Rev B. 2012;86: 054112.
[15] Shimamoto K, Hatabayashi K, Hirose Y, et al. Full compensation of oxygen vacancies in $EuTiO_3$ (001) epitaxial thin film stabilized by a $SrTiO_3$ surface protection layer. Appl Phys Lett. 2013;102:042902.
[16] Chae SC, Chang YJ, Kim D-W, et al. Magnetic properties of insulating $RTiO_3$ thin films. J Electroceram. 2009;22:216–220.
[17] Kugimiya K, Fujita K, Tanaka K, et al. Preparation and magnetic properties of oxygen deficient $EuTiO_{3\text{-}delta}$ thin films. J Magn Magn Mater. 2007;310:2268–2270.
[18] Fujita K, Wakasugi N, Murai S, et al. High-quality antiferromagnetic $EuTiO_3$ epitaxial thin films on $SrTiO_3$ prepared by pulsed laser deposition and postannealing. Appl Phys Lett. 2009;94:062512.
[19] Hatabayashi K, Hitosugi K, Hirose Y, et al. Fabrication of $EuTiO_3$ epitaxial thin films by pulsed laser deposition. Jap J Appl Phys. 2009;48:100208.
[20] Wang H-H, Fleet A, Brock JD, et al. Nearly strain-free heteroepitaxial system for fundamental studies of pulsed laser deposition: $EuTiO_3$ on $SrTiO_3$. J Appl Phys. 2004;96:5324–5328.
[21] Freeland JW, Chakhalian J, Boris AV, et al. Charge transport and magnetization profile at the interface between the correlated metal $CaRuO_3$ and the antiferromagnetic insulator $CaMnO_3$. Phys Rev B. 2010;81:094414.
[22] J.A. Woollam Co., Inc. Guide to using WVASE32: spectroscopic ellipsometry data acquisition and analysis software. Available from: http://www.jawoollam.com
[23] Menzel D, Popovich P, Kovaleva NN, et al. Electron-phonon interaction and spectral weight transfer in $Fe_{1\text{-}x}Co_xSi$. Phys Rev B. 2009;79:165111.
[24] Yu OY, Cardona M. Fundamentals of semiconductors: physics and materials properties. Berlin: Springer; 2005.
[25] Allieta M, Scavini M, Spalek LJ, et al. Role of intrinsic disorder in the structural phase transition of magnetoelectric $EuTiO_3$. Phys Rev B. 2012;85:184107.
[26] Kim J-W, Thompson P, Brown S, et al. Emergent superstructural dynamic order due to competing antiferroelectric and antiferrodistortive instabilities in bulk $EuTiO_3$. Phys Rev Lett. 2013;110:027201.
[27] Petrović AP, Kato Y, Sunku SS, et al. Electric field modulation of the tetragonal domain orientation revealed in the magnetic ground state of quantum paraelectric $EuTiO_3$. Phys Rev B. 2013;87:064103.
[28] Ellis DS, Uchiyama H, Tsutsui S, et al. X-ray study of the structural distortion in $EuTiO_3$. Physica B. 2014;442:34–38.
[29] Ellis DS, Uchiyama H, Tsutsui S, et al. Phonon softening and dispersion in $EuTiO_3$. Phys Rev B. 2012;86:220301.
[30] Reuvekamp P, Kremer R, Köhler J, et al. Spin-lattice coupling induced crossover from negative to positive magnetostriction in $EuTiO_3$. Phys Rev B. 2014;90:104105.
[31] Spalek LJ, Saxena SS, Panagopoulos C, et al. Elastic and anelastic relaxations associated with phase transitions in $EuTiO_3$. Phys Rev B. 2014;90:054119.
[32] Schiemer J, Spalek LJ, Saxena SS, et al. Magnetoelastic relaxations in $EuTiO_3$. Euro Phys Lett. 2015;109:57004.

[33] Müller KA, Burkard H. $SrTiO_3$: an intrinsic quantum paraelectric below 4 K. Phys Rev B. 1979;19:3593−3596.
[34] Köhler J, Dinnebier R, Bussmann-Holder A. Structural instability of $EuTiO_3$ from X-ray powder diffraction. Phase Transit. 2012;85:949−954.
[35] Guguchia KZ, Keller H, Kremer RK, et al. Spin-lattice coupling induced weak dynamical magnetism in $EuTiO_3$ at high temperatures. Phys Rev B. 2014;90:064413.
[36] Guguchia Z, Shengelaya A, Keller H, et al. Tuning the structural instability of $SrTiO_3$ by Eu doping: the phase diagram of $Sr_{1-x}Eu_xTiO_3$. Phys Rev B. 2012;85:134113.
[37] Geday MA, Glazer AM. Birefringence of $SrTiO_3$ at the ferroelastic phase transition. J Phys: Cond Mat. 2004;16:3303−3306.
[38] Roleder K, Bussmann-Holder A, Górny M, et al. Precursor dynamics to the structural instability in $SrTiO_3$. Phase Transit. 2012;85:939−948.
[39] Ellis DS, Uchiyama H, Tsutsui S, et al. Phonon softening and dispersion in $EuTiO_3$. Phys Rev B. 2012;86:220301.
[40] Reuvekamp P, Kremer R, Köhler J, et al. Spin-lattice coupling induced crossover from negative to positive magnetostriction in $EuTiO_3$. Phys Rev B. 2014;90:104105.
[41] Spalek LJ, Saxena SS, Panagopoulos C, et al. Elastic and anelastic relaxations associated with phase transitions in $EuTiO_3$. Phys Rev B. 2014;90:054119.
[42] Schiemer J, Spalek LJ, Saxena SS, et al. Magnetoelastic relaxations in $EuTiO_3$. Euro Phys Lett. 2015;109:57004.
[43] Bussmann-Holder A, Köhler J, Whangbo M-H. Unexpected precursor effects to the structural phase transition in $EuTiO_3$. Z Anorg All Chem. 2015;641:180−185.
[44] Schiemer J, Spalek LJ, Saxena SS, et al. The magnetic field and in-situ stress dependence of elastic behavior in $EuTiO_3$ from resonant ultrasound spectroscopy. Phys Rev B. 2016;93:054108.
[45] Ranjan R, Nabi HS, Pentcheva RJ. Electronic structure and magnetism of $EuTiO_3$: a first-principles study. J Phys Cond Mat. 2007;19:406217.
[46] Ranjan R, Nabi HS, Pentcheva RJ. First principles study of magnetism in divalent Eu perovskites. J Appl Phys. 2009;105:053905.
[47] Akamatsu H, Fujita K, Hayashi H, et al. Crystal and electronic structure and magnetic properties of divalent europium perovskite oxides $EuMO_3$ (M = Ti, Zr and Hf): experimental and first-principles approaches. Inorg Chem. 2012;51:4560−4565.
[48] Akamatsu H, Fujita K, Zong Y, et al. Impact of amorphization on the magnetic properties of EuO-TiO_2 system. Phys Rev B. 2010;82:224403.
[49] Wu H, Jiang Q, Shen WZ. Coupling between the magnetism and dielectric properties in $Eu_{1-x}Ba_xTiO_3$. Phys Rev A. 2004;69:014104.
[50] Rushchanskii KZ, Kamba S, Goian V, et al. A multiferroic material to search for the permanent electric dipole moment of the electron. Nat Mat. 2010;8:649−654.
[51] Shafer MW. Preparation and crystal chemistry of divalent europium compounds. J Appl Phys. 1965;36:1145−1150.